the flexural stress cycles seen by flaws. Transverse fissures may be driven initially by longitudinal stresses due to flexure and later by the action of the fully reversed shear stresses due to bending of the head on the web. Similarly, vertical split-head flaws may be driven by the flexural action of lateral loads, again influenced by the action of the fully reversed shear stresses. The growth of horizontal splits in the railhead appears to be dominated by shear stresses, except in the very earliest stages of growth. For horizontal flaws at depths of less than 0.76 cm the effects of transverse shear stresses due to whole-rail flexure dominate but, below this depth, the shear stresses resulting from the bending of the head on the web become increasingly significant. However, in light of the complexities of the factors that control stresses in rails, these conclusions must be considered as preliminary.

ACKNOWLEDGMENT

The results summarized in this paper were developed at Battelle Columbus Laboratories and the U.S. Department of Transportation, Transportation Systems Center, under the sponsorship of the Federal Railroad Administration. We gratefully acknowledge the contributions of P. M. McGuire, S. G. Sampath, and E. F. Rybicki of Battelle Columbus Laboratories, A. B. Perlman of Tufts University, and J. J. Lanza of the Transportation Systems Center in the conduct of the rail-stress program summarized here.

REFERENCES

1. J. J. Hitz. Track-Related Accident Causes: Phase 1. Transportation Systems Center, Cambridge, MA; Federal Railroad Administration, May 1977.
2. M. M. Frocht and B. C. Wang. A Three-Dimensional Photoelastic Study of Interior Stresses in the Head of a Railroad Rail in the Region Under a Wheel. Proc., ASME, 4th U.S. National Congress on Applied Mechanics, Berkeley, CA, Vol. 1, 1962, pp. 603-609.
3. C. J. Code. Wheel Load, Wheel Diameter, and Rail Damage. Bulletin, AREA, Vol. 59, 1960.
4. G. H. Way, Jr. Heavy Cars: What Are the Issues? Bulletin, AREA, Vol. 76, No. 653, June 1975.
5. A. D. Kerr. On the Stress and Stability Analyses of Railroad Track. ASME, Journal of Applied Mechanics, Vol. 76, No. 1, 1973, pp. 1-5.
6. D. P. McConnell. Stresses in Rails. Transportation Systems Center, Cambridge, MA, Technical Memorandum, Nov. 1976.
7. T. G. Johns and K. B. Davies. Preliminary Description of Stresses in Railroad Rail. Federal Railroad Administration, Rept. No. FRA-ORD-77-35, Nov. 1976.
8. B. Paul. A Review of Rail-Wheel Contact Stress Problems. Proc., Princeton University Symposium on Railroad Track Mechanics, Elsevier, New York, 1975.
9. R. K. Steele. Requirements for the Reliability Assessment of Railroad Rail in Service. Proc., Princeton University Symposium on Railroad Track Mechanics, Elsevier, New York, 1975.
10. T. G. Johns and others. Engineering Analysis of Stresses in Railroad Rail: Phase 1. Federal Railroad Administration, June 1977.

Analytical and Experimental Study of Residual Stresses in Rails

Kent B. Davies and Thomas G. Johns, Battelle Columbus Laboratories, Columbus, Ohio

A mathematical model for the calculation of railhead residual stresses is presented together with the results for a specific case of wheel loading. These data are then compared with the results obtained by destructive evaluation of residual stresses in simulated railhead specimens. Finally, the results obtained are compared with published values for residual stress.

New rails have an initial residual stress field that is an artifact of the mechanical working of the manufacturing process. After their installation in track, this initial stress field begins to change under the recurring plastic deformation caused by passing wheel loads. The new residual stress state that is established, which may or may not continue to change during the life of the rail, is believed to have a profound effect on the formation of railhead cracks. But because of the difficulties implicit in the analysis, few investigations of rail residual stress have been reported in the literature. Those that have appeared, however, are of great interest. The most important of these are those due to Johnson (1), Merwin and Johnson (2), Johnson and Jefferis (3), Martin and Hay (4), and the Office for Research and Experiments of the International Union of Railways (ORE) (5).

Previous approaches to the study of rail residual stresses have involved both analytical and experimental methods. Analytical techniques have been based on the application of approximate numerical methods. Experimental approaches have relied on various destructive techniques, such as sectioning out and hole drilling. Figure 1 shows the results obtained by Martin and Hay (4) for the three normal, residual stress components calculated by a method based, in part, on that presented by Johnson and coworkers (1, 2, 3). Figure 2 shows both the experimental and the analytical results obtained by ORE (5) for rail removed from service. The data presented in Figures 1 and 2 represent the only residual stress calculations that have appeared in the literature so far.

NUMERICAL ANALYSIS OF RAILHEAD RESIDUAL STRESSES

A numerical method was developed for the calculation

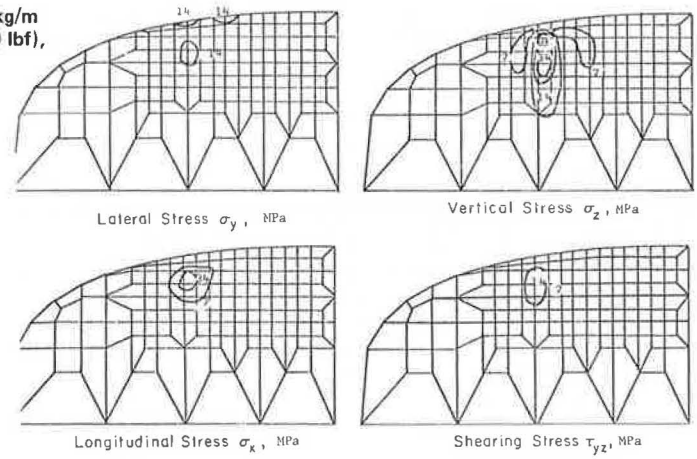

Figure 1. Residual stress components: 65.6-kg/m (132-lb/yd) RE railhead, P = 84.6 kN (19 000 lbf), and K = 379 MPa (55 000 lbf/in²).

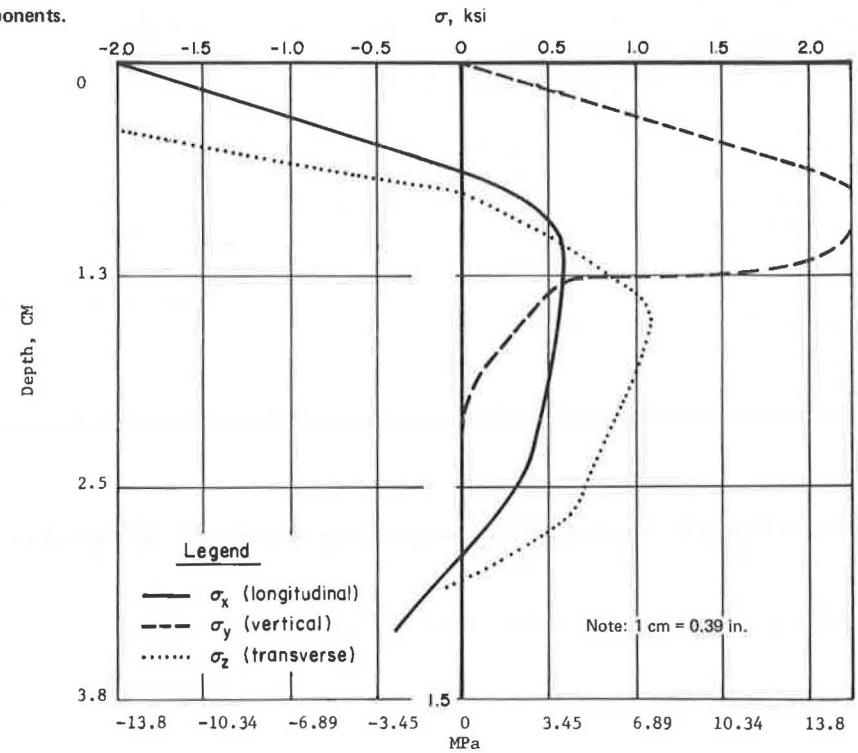

Figure 2. Experimental residual stress components.

of the residual stresses caused by wheel-rail contact. This analytical procedure extends the work of Merwin and Johnson (2) and of Martin and Hay (4) in that it is fully three dimensional (by using a direct finite-element approach) and includes the effect of work hardening.

The flow diagram shown in Figure 3 summarizes the calculation procedure. The first step in the computation is the determination of the subsurface strains by using the specified load and contact distributions and the three-dimensional finite-element model. This consisted of a quarter-section model of the railhead in which two vertical planes of symmetry were assumed. The model was a rectangular solid that had a 3x3.25-cm (1.2x 1.3-in) cross section. A constant-cross-section mesh was repeated at varying intervals along the length of the model. A cross-sectional view of the model is shown in Figure 4. It included 630 isoparametric-brick elements consisting of 1340 nodes. The loading was applied in the form of a 84.6-kN (19 000-lbf) Hertzian contact distribution having a 0.64-cm (0.27-in) semimajor axis and a 0.47-cm (0.19-in) minor axis. To avoid the additional complication of flexural stresses, the model was supported by a rigid foundation.

For the residual-stress analysis, it was necessary to construct a strain cycle that simulated the passage of a rolling load for a single cross-sectional plane. This was done from the simple static-contact cases analyzed by the finite-element method by using the GENTAPE program. It was assumed that the strain seen at any point in the railhead would be the same as that seen by any other point lying on the same longitudinal line at some time. Thus, the variation in strain along a given longitudinal line due to a static load was taken to be the same as the strain at a point as a loaded wheel passed by. The GENTAPE program assembled a magnetic tape of strain cycles for the nodal points of the cross section shown in Figure 4. The results of this compilation are shown for the elastic case in Figure 5. The elastic strain in the y-direction was compared with that determined by Martin and Hay (4) by an indirect finite-element solution, and good agreement was found

Figure 3. Flowchart of residual stress calculation procedure.

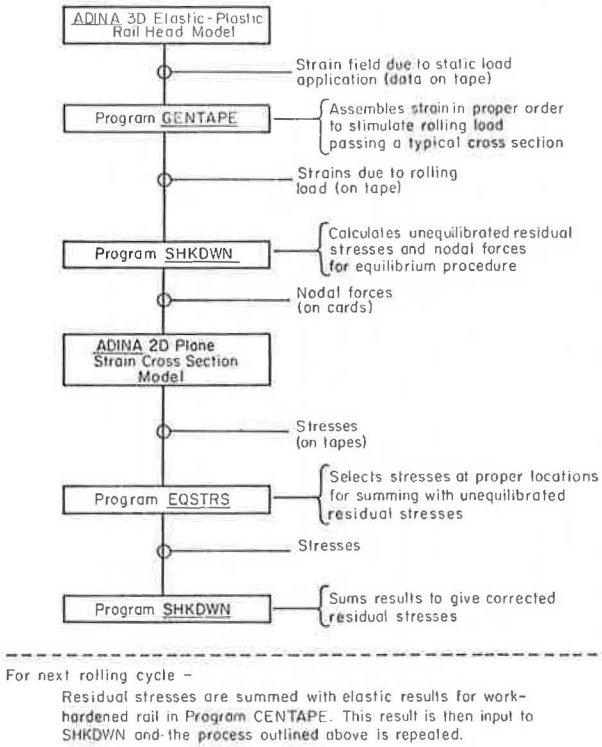

Figure 4. End-sectional view of three-dimensional finite-element grid for railhead analysis.

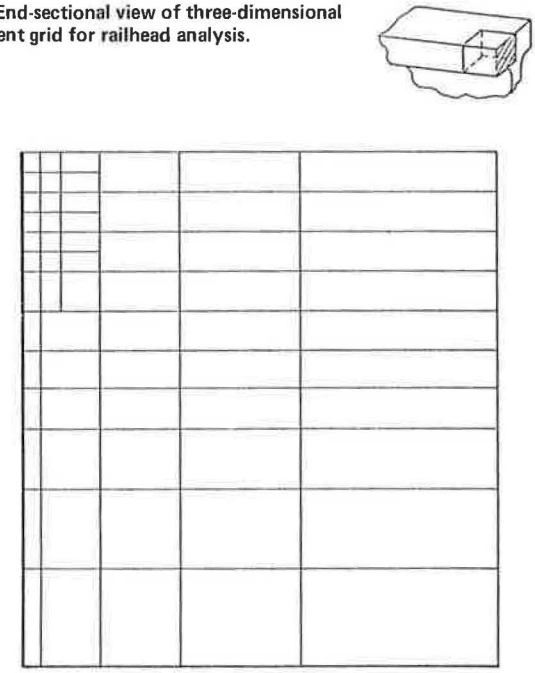

for the components. These particular strain cycles were computed for a point lying at a depth of 1.91 cm (0.75 in) below the rail surface. Similar cycles, differing only in the magnitudes of the components, exist for the other points in the plane.

The SHKDWN program calculates unequilibrated stresses on the basis of the following assumptions:

1. The elastic strain cycle that can be derived from a static-contact situation is a sufficiently close approximation to the true elastoplastic strain cycle of the rolling contact situation [as assumed by Merwin and Johnson (2)].
2. The material is isotropic and elastic-plastic and obeys an isotropic strain-hardening law. Its yielding is described by the Von Mises criterion and the Prandtl-Reuss equations.
3. Every plane of the rail remains identical to every other plane in the rail in terms of both residual stress and material properties. Thus, σ_{xz} and σ_{yx} are everywhere zero when no load is present.
4. A vertical plane of symmetry is assumed to exist on the longitudinal centerline of the rail. Thus, only half the railhead is included in the analysis.

Analysis proceeds in the program in the following manner:

1. Various problem parameters are read in, such as the coefficients of the linear equation that describes the stress-strain curve, the yield stress, Poisson's ratio, and the problem size.
2. Strain-cycle information is read from a tape on a mesh-point-by-mesh-point basis. For each increment of strain, the stresses at all of the points in the cross section are evaluated before moving on to the next increment. After the strain tensor at a point is read in, the strain components are transformed into deviatoric stress components by the relationships

$$S_{ij} = \sigma_{ij} - S_m \quad (i = j = 1, 2, 3) \tag{1}$$

where

$$S_m = \sigma_{ii}/3 \quad (i = 1, 2, 3) \tag{2}$$

At the same time, the strain-deviation gradient is calculated as a three-point divided difference approximation to the derivative. Thus,

$$\begin{aligned}(d\epsilon_{ij}/dx)|_n \cong\ & [(\epsilon_{ij}|_n - \epsilon_{ij}|_{n-1})/(x_n - x_{n-1})] + (x_n - x_{n-1}) \\ & \times [(\epsilon_{n+1} - \epsilon_n)/(x_{n+1} - x_n)] - [(\epsilon_n - \epsilon_{n-1})/(x_n - x_{n-1})] \\ & \div (x_{n+1} - x_{n-1})\end{aligned} \tag{3}$$

is the gradient at the nth point in the mesh. Finally, the equivalent strain for the current strain level is calculated by using the familiar expression

$$\begin{aligned}\epsilon_{ef} = (2/3)\,[&(\epsilon_{11} - \epsilon_{22})^2 + (\epsilon_{22} - \epsilon_{33})^2 + (\epsilon_{33} - \epsilon_{11})^2 \\ &+ (3/2)(\epsilon_{12}^2 + \epsilon_{23}^2 + \epsilon_{13}^2)]^{1/2}\end{aligned} \tag{4}$$

3. By using the results of the uniaxial stress-strain curve, the Von Mises yield criterion

$$\sigma_{ef} < \sigma_y \tag{5}$$

where σ_y = equivalent stress at yield (for the first approach to yielding) is applied. If yield has not occurred at that mesh point, the stress is merely assumed to be that given by Equation 1. The program then proceeds to the next mesh point and repeats the sequence of computations. If, however, it is found that yielding has occurred, then the increment of stress due to the current value of strain is calculated by using the Prandtl-Reuss equations. These may be written in terms of deviatoric stress and strain. Specifically, the time rate of change visually indicated is replaced by the gradient in the rolling direction so that

Figure 5. Elastic strains along rail axis due to 84.6-kN (19 000-lbf) load: longitudinal plane of symmetry and depth of 1.91 mm (0.075 in).

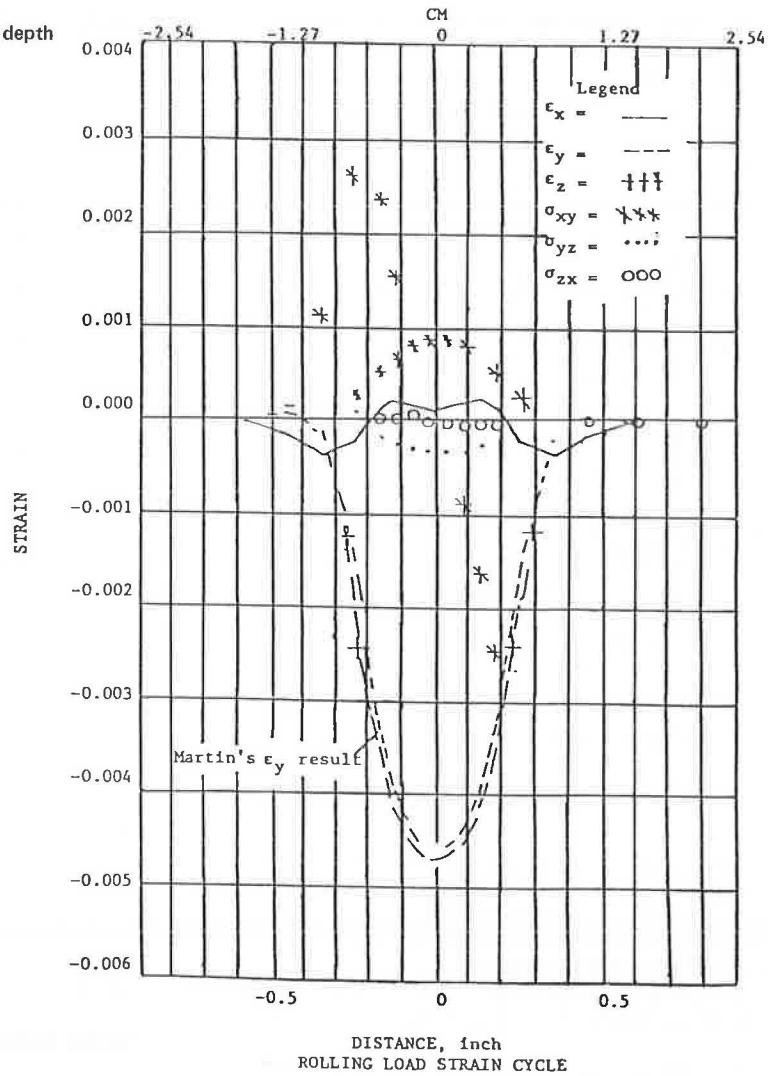

$$(\Delta S_x/\Delta x) = 2G[(\Delta\epsilon_x/\Delta x) - (\Delta W\Delta x^{-1}/K^2)S_x]$$
$$(\Delta S_y/\Delta x) = 2G[(\Delta\epsilon_y/\Delta x) - (\Delta W\Delta x^{-1}/K^2)S_y]$$
$$(\Delta S_z/\Delta x) = 2G[(\Delta\epsilon_z/\Delta x) - (\Delta W\Delta x^{-1}/K^2)S_z]$$
$$(\Delta\tau_{xz}/\Delta x) = G[(\Delta\gamma_{xz}/\Delta x) - (\Delta W\Delta x^{-1}/K^2)\tau_{xz}]$$
$$(\Delta\tau_{xy}/\Delta x) = G[(\Delta\gamma_{xy}/\Delta x) - (\Delta W\Delta x^{-1}/K^2)\tau_{xy}]$$
$$(\Delta\tau_{yz}/\Delta x) = G[(\Delta\gamma_{yz}/\Delta x) - (\Delta W\Delta x^{-1}/K^2)\tau_{yz}] \tag{6}$$

where $\Delta W/\Delta x$ = rate of plastic work and is given by

$$(\Delta W/\Delta x) = S_x(\Delta\epsilon_x/\Delta x) + S_y(\Delta\epsilon_y/\Delta x) + S_z(\Delta\epsilon_z/\Delta x) + \tau_{xy}(\Delta\delta_{xy}/\Delta x) + \tau_{yz}(\Delta\delta_{yz}/\Delta x) \tag{7}$$

and K, γ, τ, and δ have their customary meanings.

Equation 6 is the form of the Prandtl-Reuss relationship actually used in the program. The strain rates used for a particular point in the strain cycle were those given by Equation 3. The increments of stress computed by using Equation 6 are then added to the stresses computed at the previous increment of strain. This process continues during the strain cycle until unloading of a point occurs. After this, stress is again calculated elastically and further unloading proceeds elastically.

4. When the strain cycle has been completed, a system of compatible residual stresses remains. However, because the stresses at the various levels have been computed independently of each other, equilibrium is not satisfied. To remedy this, the resultant planar nodal forces are calculated that would give rise to the system of stresses just calculated if considered with respect to an assumed finite-element mesh. This is accomplished by integrating the equation of equilibrium over the indicated elements. Thus, the forces at the center of the element are given by

$$F_y = \int\int[(\partial\sigma_{yy}/\partial y) + (\partial\sigma_{yz}/\partial z)]\,dydz \tag{8}$$

and

$$F_z = \int\int[(\partial\sigma_{zz}/\partial z) + (\partial\sigma_{yz}/\partial y)]\,dydz$$

These resultant forces are apportioned equally to the four corner nodes of the assumed finite-element mesh. (The actual program is somewhat more involved than this, but the mechanical details, involved as they are with the finite-element method, will not be further elaborated upon. Nodal forces representing the residual stress system are finally output on punched cards.)

The two-dimensional, finite-element railhead cross-section model, which is exactly the same as the cross section of the three-dimensional railhead model, has 53 linear elements. The boundary conditions are appropriately arranged to simulate railhead support as described above. The analyses are performed by using the nodal forces produced from the unequilibrated residual stresses by the SHKDWN program. The resulting

stresses are output on tape.

The EQSTR program, which is structurally almost identical to the GENTAPE program, arranges the stress output from the two-dimensional finite-element model in a sequence that corresponds to that of the mesh points in the SHKDWN program. (Once again, this program is of little interest from a mechanical standpoint, so it will not be discussed further.)

The stress computation procedure is then completed by subtracting the stresses computed by the finite-element model (representing the unequilibrated portion of the computed stresses) from the original residual stress. Thus, at each mesh point

$$S_{ij}|_k = S_{ij}^{ur}|_k - S_{ij}^{fe}|_k \tag{9}$$

when $S_{ij}^{fe}|_k$ = finite-element component at the kth mesh point. The resulting stress deviations are then output as the final residual stress state for that load pass. This operation is also accomplished by using the SHKDWN program. A similar procedure is followed for the next pass of the load.

APPLICATION OF NUMERICAL METHOD TO CASE OF WHEEL-RAIL CONTACT

By using the computation procedure described above, residual stresses were calculated for the case of a 84.6-kN load on a rail modeled by a bilinear stress-strain curve that had a yield stress of 440 MPa (64 000 lbf/in^2). The stress cycle used was that described above and shown in Figure 5.

The results for one pass of the load are shown in Figure 13 of the preceding paper in this Record for the three normal stress components. It is observed that the respective maxima occurred below the surface of the rail. The vertical stress component is zero at the surface and tensile below the surface and reaches its maximum at a depth of about 2.5 mm (0.1 in). The other two normal stress components have compressive maxima and occur at somewhat shallower depths in the railhead. All of the components decay to insignificant levels at depths below 1.25 cm (0.5 in).

COMPARISON OF NUMERICAL AND EXPERIMENTAL RESIDUAL STRESS RESULTS

A destructive experimental determination of rail residual stresses was performed on simulated rail specimens that had been subjected to known rolling loads. Specimens were subjected to one or three passes of the wheel load.

The simulated specimens consisted of 25.4-cm (10.0-in) crown-radius head sections machined from a 79.5-kg (175-lb) crane-rail section. The resulting specimens were thoroughly stress relieved to eliminate any initial residual stress field. After rolling in a rolling-load machine, each specimen was dissected by using the Battelle Columbus Laboratories' sectioning technique for the determination of the three-dimensional residual stress field (6). The results from the experimental residual stress investigation are also shown in Figure 13 of the preceding paper in this Record. The rolling-load test specimens had a yield stress of 326 MPa (47 300 lbf/in^2). The specimens were loaded to a level of 64.5 kN (14 500 lbf). If the two sets of properties and loads are considered in relation to each other, it is seen that the laboratory specimen was the more severely loaded. By using the ratio of the maximum contact pressure to the shear yield stress as a means of comparison (1), it is found that the mathematically modeled case had a ratio (R) of 4.1116 and the laboratory case had R = 6.1616. Thus, it would be expected that the residual stress formation would be more developed in the experimentally measured case. Examination of the plot of longitudinal stresses shows that the results predicted by the model are slightly larger than the experimental results. In addition, the effects occur somewhat more shallowly in the model. The transverse stress results show the expected trend; the laboratory stresses are the larger and occur at the greater depth. Examination of the vertical stress results shows very poor agreement. At this time, no rationale can be offered for this disparity. It is interesting to note that, in the case of the horizontal plane stress components, the greatest difference between the one-pass and the three-pass specimens occurred on the surface. Thus, it was concluded that, with the exception of the vertical stress, there was reasonably good agreement between the mathematical model and the laboratory validation experiments when the strain cycle was assumed to be an elastic one.

COMPARISON WITH PUBLISHED RESULTS AND CONCLUSIONS

A mathematical model of residual stress formation in railroad rails was developed. The results obtained by using this numerical method were in reasonable agreement with the experimentally determined values obtained in this study. It is useful to compare these results with data published in the literature.

The experimental and analytical results can be most conveniently compared with those obtained by ORE (5). Such a comparison is made difficult by the fact that the ORE work was conducted on rail removed from service that had a tensile yield strength of approximately 689 MPa (100 000 lbf/in^2). Thus, the situation analyzed here was significantly different than that reported by ORE.

Comparison of the vertical stress results shows that the tensile maximum in the specimens examined by ORE was located at a depth approximately 0.62 cm (0.25 in) lower than the tensile maximum in the analytical results. Although this component is also about 34.5 MPa (5000 lbf/in^2) greater in magnitude, the agreement is considered measurable. The ORE curve disagrees with the experimental curves. Martin and Hay (4) showed a tensile maximum of about 68.9 MPa.

Comparison of the transverse component results shows several differences between the analytical results and those reported by ORE. The tensile maximum occurs at a considerably greater depth, and a very high compressive value is indicated at the surface of the rail.

The longitudinal residual stress results showed better agreement, although the ORE maximum once again occurred somewhat deeper in the railhead. Once again, the high compressive stress reported on the running surface by ORE was not found in our work.

Despite the degree of success with which it predicted residual stress magnitude, the model is sufficiently complex to make the calculation of the effect of many cycles of the load application both difficult and costly. Thus, it is recommended that future residual stress determinations be carried out experimentally by using rail removed from service for which the service history is accurately known.

ACKNOWLEDGMENTS

This work was supported by the Federal Railway Administration. We are pleased to acknowledge the assistance in all phases of the program of Donald McConnell of the U.S. Department of Transportation, Transportation Systems Center. Jack Groom was responsible for con-

ducting the experimental work reported in this paper.

REFERENCES

1. K. L. Johnson. A Shakedown Limit in Rolling Contact. Proc., ASME, 4th U.S. National Congress on Applied Mechanics, Berkeley, CA, Vol. 1, 1962, pp. 971-975.
2. J. E. Merwin and K. L. Johnson. An Analysis of Plastic Deformation in Rolling Contact. Proc., Symposium on Fatigue in Rolling Contact, Institute of Mechanical Engineers (London), Vol. 177, No. 24, 1963, pp. 676-688.
3. K. L. Johnson and J. A. Jefferis. Plastic Flow and Residual Stresses in Rolling and Sliding Contact. Proc., Symposium on Fatigue in Rolling Contact, Institute of Mechanical Engineers (London), Vol. 177, 1963, p. 95.
4. G. C. Martin and W. W. Hay. The Influence of Wheel-Rail Contact Forces on the Formation of Rail Shells. Trans., ASME, 72-WA/RT-8, 1972.
5. Study of Fatigue Phenomena of the Rail in the Contact Zone With the Wheel. Office for Research and Experiments of the International Union of Railways, Rail International, Vol. 3, No. 13, Sept. 1973, pp. 741-794.
6. T. G. Johns and others. Engineering Analysis of Stresses in Railroad Rail: Phase 1. Federal Railroad Administration, June 1977.

Mathematical Model for Lateral Thermal Buckling and Displacement of Curved Track

W. So, Research and Test Department, Association of American Railroads, Chicago
W. W. Yang, Consolidated Rail Corporation, Chicago

One disadvantage of continuously welded rails is that the possibility of track buckling because of temperature increases is increased significantly by the elimination of rail joints. Many mathematical models have been developed for the buckling of tangent tracks, but there are very few that deal with curved tracks. The objective of this paper is the development of methods for the prediction of both the lateral thermal-buckling load and the corresponding displacement of curved tracks so that criteria for track design, maintenance, and evaluation can be formulated. This objective has been achieved by using a two-dimensional finite-element model that simulates the lateral stability of a track subjected to temperature increases and train wheel loads. This paper illustrates only the basic applications and the potential of the model. A parameter investigation was made that included tracks that had curvatures varying from 0 to 10° and studied the effects of various track parameters on the buckling temperature and the lateral track displacement. The results indicate that the buckling temperature and lateral displacement of a curved track are significantly affected by changes in lateral ballast resistance, misalignment and curvature, and by the presence of ineffective ties. The model provides a promising new approach to the track-buckling problem; however, test data are needed to validate it.

Continuously welded rail is being increasingly used in railway track construction in the United States. A well-known disadvantage of such rails is that the possibility of track buckling because of temperature increases is increased significantly by the elimination of rail joints. Derailments attributed to track buckling have been reported (1). This track-buckling problem—also called the track-stability problem—is consequently of great importance on continuously welded tracks.

Track stability can be subdivided into two main categories according to the plane in which buckling occurs: lateral and vertical. Lateral stability refers to buckling that occurs in the plane of the track, and vertical stability refers to the uplift of the track. Vertical buckling is unlikely to occur, because the initial uplift of the track reduces the lateral ballast resistance and usually causes lateral buckling.

Many mathematical models have been developed for the lateral stability of tangent track, but there are very few that deal with curved track. The objective of this paper is the development of methods for the prediction of both the lateral thermal-buckling load and the corresponding displacement of curved track so that criteria for track design, maintenance, and evaluation can be formulated. This objective is achieved by using a two-dimensional finite-element model that simulates the lateral stability of a track subjected to temperature increases and train wheel loads.

The model was first developed by So and Martin (2) to solve the problem of the lateral stability of tangent tracks. Reasonably good agreement was obtained between the model results and test data. There are no other known applications of finite-element models in this respect. Previous applications of the finite-element method in the analysis of tracks were primarily for the calculation of stresses in the rails under wheel loads.

The finite-element model is quite powerful and efficient in simulating track stability because it uses standard structural-analysis computer programs for elastic frames. A remarkable advantage of the model is its versatility in incorporating all the main parameters that govern the lateral stability of track (3): (a) condition of lateral rail support, (b) rotational resistance of rail fasteners, (c) flexural rigidity of rails, (d) track curvature, (e) track irregularities (such as misalignments and ineffective ties or rail fasteners), and (f) loading on the track (such as thermal loads due to heating of the rails; vertical, lateral, and longitudinal loads due to normal traffic; dynamic vibrations; and train braking and acceleration). Longitudinal loading here refers to loading along the rails. The model uses geometrically nonlinear-beam-deflection theory (large-deflection theory). Geometrically linear-beam-deflection theory (small-deflection theory) has been used for track-